Supporting Information for "Elucidating large-scale atmospheric controls on Bering Strait throughflow variability using a data-constrained ocean model and its adjoint"

An T. Nguyen[1], Rebecca A. Woodgate[2], and Patrick Heimbach[1]

[1]University of Texas at Austin, Austin, TX, USA

[2]University of Washington, Seattle, WA, USA

Contents of this file

1. Dependence of reconstruction of $\widetilde{\delta J}$ on the time when J is defined
2. Reconstruction: temporal component derivations
3. Figures S1–S3

Introduction

The materials included here (i) clarify the choice of the timing of when the quantity of interest, i.e. the Bering Strait transport, is defined, and (ii) provide of full derivation of the formulation used to decompose the Bering Strait transport anomaly time-series into temporal components.

1. Dependence of reconstruction of $\widetilde{\delta J}$ on the time when J is defined

The monthly mean transport $J(t_i)$ for each month t_i has large variability with negative values (southward flow) during some months and maximum positive values during other months (Fig. S1a). An important question is whether and how the gradients $\frac{\partial J}{\partial \Omega_k}$ vary when J varies. Intuitively we expect that if there is a dominant linear mechanism controlling the transport, the gradient $\frac{\partial J}{\partial \Omega_k}$ retains the same sign and similar magnitude, independent of the period over which J is defined. For example, if northward wind stress is the dominant controlling mechanism such that $\frac{\partial J}{\partial \tau_N} = X$, a smaller J is then a result of weaker τ_N and a negative J is a result of a reversal of the wind stress (negative τ_N). Thus, J can vary widely and is a result of the variation in τ_N, while the physical connection, as captured by $\frac{\partial J}{\partial \tau_N} = X$, remains the same.

Following this line of argument, we hypothesize that if instead $\frac{\partial J}{\partial \Omega_k}$ is dependent on the time when J is defined (e.g., phase of the seasonal cycle), it is due to J being a highly nonlinear function of Ω_k along the model trajectory such that at any given time the linearized gradients $\frac{\partial J}{\partial \Omega_k}$ cannot fully capture the physics. We can test this dependency by comparing gradients computed from different J for each forcing variable. Most importantly, we can compare the reconstructed $\widetilde{\delta J}$ using the corresponding gradients to see the impact of varying J on the reconstructed time series.

Gradients $\frac{\partial J}{\partial \Omega_k}$ were obtained from $J^{[07,09,12]}$ for three different averaged months that span the seasonal cycle [Jul/2013, Sep/2013, Dec/2013], and each was used to reconstruct the respective time-series $\widetilde{\delta J}^{[07,09,12]}$. These constructions as well as the forward anomaly time-series δJ_{fwd} are shown in Fig. S1. Linear fit of scatter plot of these various $\widetilde{\delta J}$ show

that they are different by up to **only 3%**, depending on the number of lags used in the reconstruction (Fig. S1b,c).

Thus, given that any of the reconstructed $\widetilde{\delta J}^{[07,09,12]}$ can capture the variability in the forward model δJ_{fwd} (Fig. S1a), that the difference between the these reconstructions is small, and that subsequent analyses show no significant differences in the behavior of how the reconstructions differ from the forward model time-series (Fig. S2), as discussed in the main text, we chose J^{09} for all gradients calculations and analyses in this study.

2. Reconstruction: temporal component derivations

Eqn. (3) can be used to reconstruct the full anomaly time series, $\widetilde{\delta J}$, which can then be decomposed into temporal components associated with interannual, seasonal, and monthly time-scales, as discussed in Section 3. Here we show that by rewriting eqn. (3), the reconstruction can be **approximated** as eqn. (4), which allows for more direct connection between the time-scales of the forcing anomalies and the time-scales of the Bering Strait transport anomalies. Our example here is for the reconstruction of the annual mean time series, but the same logic applies to other time-scales.

We first define the annual mean forcing $\delta\Omega_y$ for a year t_a within the time range $[t_a, t_a+T_y]$ as,

$$\delta\Omega_y(t_a) = \frac{1}{T_y}\int_{t_a}^{t_a+T_y} \delta\Omega(t)\, dt \tag{S.1}$$

where T_y is a time period of 1 year. Based on eqn. (3), the full reconstruction for the annual $\widetilde{\delta J}_y$ for the same year t_a at a specific geographic location $[x_1, x_2]$ for a forcing component k would be as follows, where for clarity we will omit the geographic integrals and location $[x_1, x_2]$ as well as the forcing index k from the equations, but the reader should

understand these integrals are still required. Note also that the sensitivity corresponding to the first month $\frac{\partial J}{\partial \Omega(0)}$, i.e., where ($\alpha - t = 0$ mo), also termed the "zero-lag", is the average of sensitivities accumulated between 0–1 month).

$$
\begin{aligned}
&\widetilde{\delta J}_y(t_a) \qquad\qquad\qquad\qquad\qquad\qquad\qquad\qquad\qquad\qquad\qquad\qquad\qquad\qquad\qquad\qquad \text{(S.2)}\\
&= \tfrac{1}{T_y}\int_{t_a}^{t_a+T_y}\left[\int_{t_0}^{t}\tfrac{\partial J}{\partial \Omega}(\alpha - t)\delta\Omega(\alpha)d\alpha\right]dt\\
&= \tfrac{1}{T_y}\int_{t_a}^{t_a+T_y}\left[\tfrac{\partial J}{\partial \Omega}(0)\delta\Omega(t) + \int_{t_0}^{t-1mo}\tfrac{\partial J}{\partial \Omega}(\alpha - t)\delta\Omega(\alpha)d\alpha\right]dt\\
&= \tfrac{1}{T_y}\int_{t_a}^{t_a+T_y}\left[\tfrac{\partial J}{\partial \Omega}(0)\delta\Omega(t)\right]dt + \tfrac{1}{T_y}\int_{t_a}^{t_a+T_y}\left[\int_{t_0}^{t-1mo}\tfrac{\partial J}{\partial \Omega}(\alpha - t)\delta\Omega(\alpha)d\alpha\right]dt\\
&= \tfrac{\partial J}{\partial \Omega}(0)\tfrac{1}{T_y}\int_{t_a}^{t_a+T_y}\delta\Omega(t)dt + \tfrac{1}{T_y}\int_{t_a}^{t_a+T_y}\left[\int_{t_0}^{t-1mo}\tfrac{\partial J}{\partial \Omega}(\alpha - t)\delta\Omega(\alpha)d\alpha\right]dt\\
&= \tfrac{\partial J}{\partial \Omega}(0)\delta\Omega_y(t_a) + \tfrac{1}{T_y}\int_{t_a}^{t_a+T_y}\left[\int_{t_0}^{t-1mo}\tfrac{\partial J}{\partial \Omega}(\alpha - t)\delta\Omega(\alpha)d\alpha\right]dt\\
&= \tfrac{\partial J}{\partial \Omega}(0)\delta\Omega_y(t_a) + \text{other terms}
\end{aligned}
$$

The key rearrangement in this long derivation for the annual $\widetilde{\delta J}_y$ is in the forcing anomalies $\delta\Omega$, which first appear in eqn. (S.2) as the total (i.e. un-decomposed) anomalies $\delta\Omega(\alpha)$ but by the end are in the form of the yearly anomalies $\delta\Omega_y$. With more effort, we can continue to rearrange the "other terms" in the last line of eqn. (S.2) to get the equation into the form:

$$
\begin{aligned}
&\widetilde{\delta J}_y(t_a) \qquad\qquad\qquad\qquad\qquad\qquad\qquad\qquad\qquad\qquad\qquad\qquad\qquad\qquad\qquad\qquad \text{(S.3)}\\
&= \tfrac{\partial J}{\partial \Omega}(0)\delta\Omega_y(t_a) + \tfrac{\partial J}{\partial \Omega}(1)\delta\Omega_y(t_a) + ... + \tfrac{\partial J}{\partial \Omega}(11)\delta\Omega_y(t_a)\\
&+\tfrac{\partial J}{\partial \Omega}(12)\delta\Omega_y(t_a - 1) + \tfrac{\partial J}{\partial \Omega}(13)\delta\Omega_y(t_a - 1) + ... + \tfrac{\partial J}{\partial \Omega}(23)\delta\Omega_y(t_a - 1)\\
&+\text{higher lag terms}
\end{aligned}
$$

where the vector $\delta\Omega_y$ that enters into eqn. (S.3) is a **monthly** time-series and has in the last twelve entries the same $\Omega_y(t_a)$ for the year of the reconstruction t_a, followed by

$\Omega_y(t_a - 1)$ of the prior year in the previous twelve entries, and so on. Now re-expressing eqn. (S.3) in the integral form and generalizing it to time t, we obtain:

$$\widetilde{\delta J}_y(t) = \int_{t_0}^{t} \frac{\partial J}{\partial \Omega}(\alpha - t)\delta\Omega_y(\alpha)d\alpha + \text{residuals} \tag{S.4}$$

Finally, with the inclusion of the geographic integrals eqn. (S.4) becomes

$$\widetilde{\delta J}_y(t) \tag{S.5}$$
$$= \int_{t_0}^{t}\int_{x_1}\int_{x_2} \tfrac{\partial J}{\partial \Omega}(x_1, x_2, \alpha - t)\delta\Omega_y(x_1, x_2, \alpha)dx_1dx_2d\alpha + \text{residuals}$$
$$\approx \int_{t_0}^{t}\int_{x_1}\int_{x_2} \tfrac{\partial J}{\partial \Omega}(x_1, x_2, \alpha - t)\delta\Omega_y(x_1, x_2, \alpha)dx_1dx_2d\alpha$$

Eqn. (S.5) is identical to eqn. (S.2) when the "residuals" are fully taken into account, and is a good approximation of eqn. (S.2) only if the "residuals" are small. To test if the "residual" in eqn. (S.5) are indeed small for the Bering transport anomaly reconstruction, we performed reconstructions of $\widetilde{\delta J}_{[y,c,res]}$, based on either the temporal decomposition of the full reconstructed $\widetilde{\delta J}$, eqn. (3), into annual, seasonal and monthly components, which we refer to as the "exact" method, or using eqn. (4), which we refer to as the "approx" method. Results are summarized in Fig. S3. In general, regardless of the method use, the reconstructed time-series $\widetilde{\delta J}_{approx}$ and $\widetilde{\delta J}_{exact}$ capture between 80–97% of the forward signal δJ_{fwd}. Up to 12-month lag, results of the temporal decomposition from the two methods are very similar. Beyond 12-month lags, some difference can be seen with the "exact" method capturing slightly less of the explained variance at seasonal and monthly time-scales (Fig. S3f,i).

The reformulation of the reconstruction following eqn. (S.5) and eqn. (4) now allows us to quantify the interannual, seasonal, and monthly transport anomalies directly from the components of the input forcing. See discussion in Section 3 for how this second "approx" method is used to investigate the direct relationship between extreme annual forcing wind stress anomalies and extrema in Bering Strait transport anomalies.

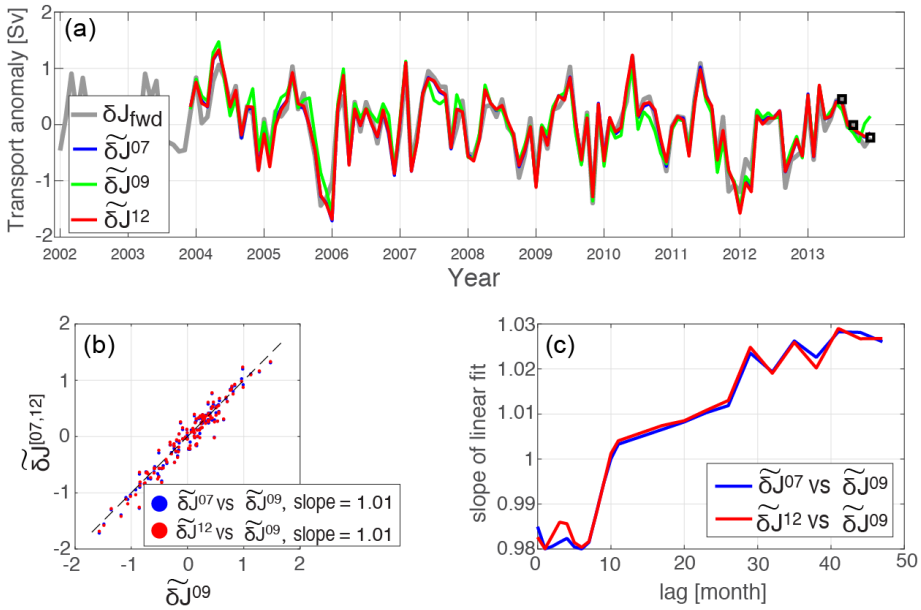

Figure S1. (a) Time-series of the transport anomaly from the forward model run (δJ_{fw}, thick gray) and the three different reconstruction ($\widetilde{\delta J}^{[07,09,12]}$) based on the sensitivity calculated from J of Jul/2013, Sep/2013, Dec/2013. The black squares are the values of $\delta J^{[07,09,12]}$. Reconstructions are summed over 24-month lags. (b) Scatter plots of reconstructed transport anomalies $\widetilde{\delta J}^{[07,12]}$ versus $\widetilde{\delta J}^{09}$, reconstructed using lags of up to 24 months. Values shown in the legend are the slope of the linear fit. (c) Slope of the linear fit using reconstructions summed up to lags ranging from 0–48months.

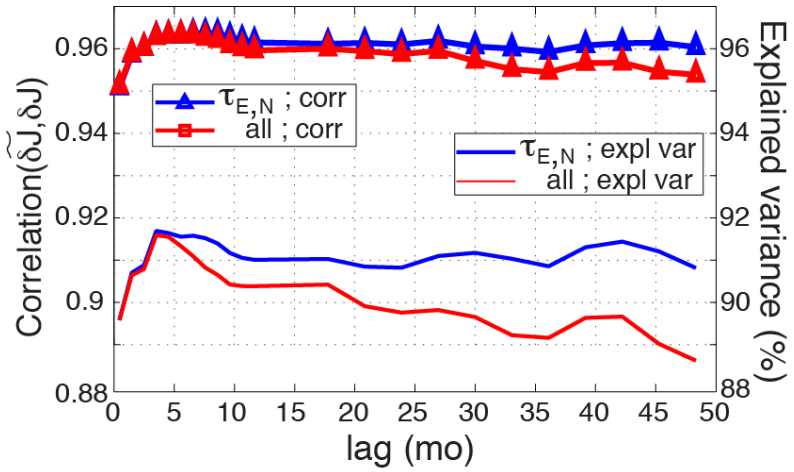

Figure S2. Correlation and explained variance as a function of lags for reconstructed $\widetilde{\delta J}^{07}$, to be compared with Fig. 3b which was obtained with $\widetilde{\delta J}^{09}$. The behavior of the correlation and explained variance are the same regardless of the choice of $J^{[07,09,12]}$ used in the computation of the gradients and the subsequent reconstructed $\widetilde{\delta J}$.

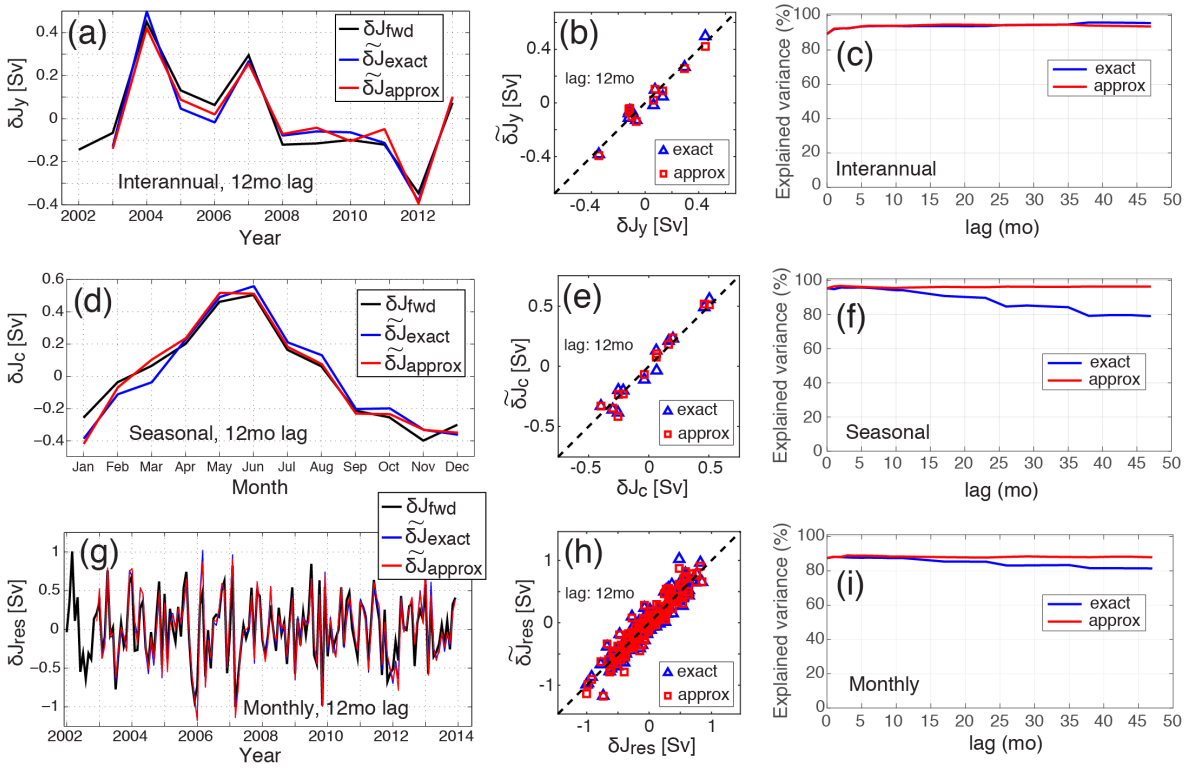

Figure S3. Comparison of $\widetilde{\delta J}_{[y,c,res]}$ using methods "exact" versus "approx". The rows correspond to (a,b,c) interannual, (d,e,f) seasonal, and (g,h,i) monthly residual decompositions. The first column (a,d,g) compared time-series of $\widetilde{\delta J}$ using the two methods against the forward time series δJ_{fwd}. The second column (b,e,h) shows scatter plots of $\widetilde{\delta J}_{approx}$ versus $\widetilde{\delta J}_{exact}$ using lags of up to 12 months. The last column (c,f,i) shows the percentage of explained variance of each reconstructed $\widetilde{\delta J}$ relative to the forward time series δJ_{fwd} for all lags.